MDPI

Article

Shock-Induced Vibration of Composite Truss Core Sandwich Plates with Distributed Nonlinear Absorbers by Optimal Locations

Wei Zhang [1], Weixing Zhang [1], Zhong Luo [2], Jianen Chen [3] and Xiangying Guo [1,*]

[1] Beijing Key Laboratory of Nonlinear Vibrations and Strength of Mechanical Structures, Faculty of Materials and Manufacturing, Beijing University of Technology, Beijing 100124, China
[2] School of Mechanical Engineering and Automation, Northeastern University, Shenyang 110819, China
[3] School of Mechanical Engineering, Tianjin University of Technology, Tianjin 300384, China
[*] Correspondence: guoxy@bjut.edu.cn

Abstract: In order to solve the problems of limited installation space and strict additional quality, the effects of internal distributed nonlinear energy sinks (NES) considering optimal locations on a composite truss core sandwich plate are investigated in this paper. Choose five NESs here and inset them in the different places of the sandwich plate to suppress the vibration of the plate, which is excited by a half-wave shock. The coupled dynamic equations of the system are derived by the principle of conservation of energy. Then, the vibration-control performances of five NESs are discussed by numerical simulation. The distributions of the five NESs are analyzed, and the optimal position distributions are obtained. Based on the optimal location, the transient responses of the system are studied. Moreover, the performances of five NESs and a single NES are compared in different dimensions. Finally, it is found that the selection of parameters has a great impact on the effectiveness of the five NESs. The new distribution way is introduced to improve the suppression effects of the five NESs in the sandwich plate.

Keywords: composite truss core sandwich plate; nonlinear energy sinks; vibration reduction; distribution

1. Introduction

Sandwich structures are usually composed of two stiff face skins and a thicker core material, such as Kagome, tetrahedral, and pyramidal cores. They have a broad application prospect in the engineering field because of their excellent properties, such as high specific strength, high specific stiffness, energy absorption, thermal conductivity, and so on [1–4].

In recent years, many scholars have done a lot on sandwich structures to grasp their characteristics more. Zhang et al. [5] investigated the global and chaotic dynamics of sandwich plates with truss core. Wang et al. [6] studied the acoustic transmission of laminated composite sandwich structures with pyramidal truss cores. Zangana et al. [7] analyzed the dynamic characteristics of composite corrugated core sandwich structures subjected to low-velocity shocks. Lou et al. [8] theoretically and experimentally investigated the natural frequencies and the vibration modes of pyramidal truss core sandwich structures with local damage. Xiong et al. [9] analyzed the structural performance of composite sandwich panels under direct shear and three-point bending loads. Wang et al. [10] investigated the mechanical behaviors of composite sandwich plates with 2-D lattice truss cores by out-of-plane compression, shear, and three-point bending tests. Huang et al. [11] analyzed the dynamic responses and failures of composite lattice core sandwich beams under impulsive loading. In addition, considering the special core layer of the sandwich structures, some scholars, such as Yin et al. [12], investigated their internal space availability. They analyzed the damping performance and energy absorption capacity of silicone rubber-filled sandwich structures. Zhang et al. [13] studied the dynamic responses of pyramidal

lattice core sandwich panels, improving the energy absorption and low-velocity shock resistances by filling the polyurethane foams. Chen et al. [14] put forward the aerogel-filled sandwich panels to provide both mechanical supports and thermal insulation.

Meanwhile, vibration control is another important research topic of sandwich structures, specifically in the condition of strong reliability and high vibration-suppression requisition. Li et al. [15] analyzed the vibration-suppression effects of the active control method on the vibration responses of lattice sandwich beams by the piezoelectric actuator/sensor pairs. Song et al. [16] analyzed the flutter suppression of the lattice sandwich beams by means of active vibration control. Chai et al. [17] investigated the nonlinear dynamic responses and vibration control of sandwich plates with different cores.

As a passive vibration-control device, nonlinear energy sink (NES) has great advantages in controlling the vibration of structures, such as a small additional mass, a wider vibration-suppression frequency band, and targeted energy transfer [18–22]. In order to make NES better serve the structures, many scholars have done a lot of research on it. Moslemi et al. [23] analyzed the effects of NES on the dynamic responses for axially moving beams. Liu et al. [24] investigated the vibration-suppression efficiency of NES with geometrically nonlinear damping. Taghipour et al. [25] researched the steady-state dynamic responses of a primary structure with cubic nonlinear stiffness connected with an NES under harmonic excitations. Fang et al. [26] analyzed the vibration-suppression of bistable NES on the transient responses of a Bernoulli–Euler beam and targeted energy transfer of the system. Zang et al. [27] discussed the influence of lever-type NES on the dynamic responses of structures subjected to harmonic excitation. Tian et al. [28] attached NES to a hypersonic 3-D wing to reduce the aeroelastic responses of a wing. Li et al. [29] proposed a symmetric single-sided vibro-impact NES to suppress the vibration of cantilever beams. Zhang et al. [30] used an NES to rapidly suppress the transient vibration of an axially moving beam. Yao et al. [31] discussed the effects of a grounded NES on the lateral vibration of rotor systems. Chen et al. [32] obtained better vibration reduction by comparing parallel NESs with a single one. They also found that the parallel NES could eliminate the higher branch responses of the system due to nonlinear terms. Wei et al. [33] improved the targeted energy transfer efficiency of NES by paralleling two different types of NES. Zhang et al. [34] studied the dynamic responses of the axially moving beam with parallel NES. Ding et al. [35,36] realized the effective suppression of structural vibration through boundary NES. In addition, Ding et al. [37,38] also studied the optimal design criteria of NES to expand the application scope of NES.

With the increasingly complex service environment of the structures, the requirements for vibration control are becoming stricter, and NES can be used as an effective device to quickly suppress the vibration of composite truss core sandwich plates. In addition, although many studies have been carried out on NES, the existing studies rarely consider the optimal location distributions of multiple NESs on the continuum. This paper presents the vibration-control performances of internal multiple NES absorbers, considering optimal locations on a composite truss core sandwich plate with shock loading. Firstly, the dynamical equations of motion for a composite truss core sandwich plate are built with five inside-distributed NESs. These NESs are embedded in the core of the sandwich plate, where one NES is in the center of the composite plate and the other four NESs are symmetrically placed on four sides of the plate. Then, the influences of the position distribution of the NESs on the energy dissipation capacity are discussed. Based on the criteria of the optimal energy dissipation position, the feasibility of the scheme and the difference of the vibration reduction of the first three modes of the sandwich plate are analyzed by the transient response. In addition, the vibration-control performances of the single NES and the distributed five NESs are compared to show the suppression advantages of the five NESs with the same structure. Finally, the effects of different parameters for the five NESs on energy dissipation are investigated to improve the performance of the distributed nonlinear absorbers.

2. Equation of Motion

Consider a composite truss core sandwich plate subjected to a shock load *F* as in Figure 1a. The sandwich plate is composed of three layers, where the upper and lower face sheets are made of carbon fibers and the middle core is arranged by pyramidal truss core. The five NESs are named as N_1, N_2, N_3, N_4, and N_5, respectively, which are embedded in five different truss core units. The pyramidal truss core unit with the NES is shown in Figure 1b. The mechanical model of the NES is shown in Figure 1c. A Cartesian coordinate system is built in the middle surface of the plate, and *u*, *v*, and *w* represent the displacements of any point of the plate in the *x*, *y*, and *z* directions, respectively. The shock load *F* acts on the position (P_1, P_2). Moreover, the symbolic representation of structural parameters is shown in Table 1.
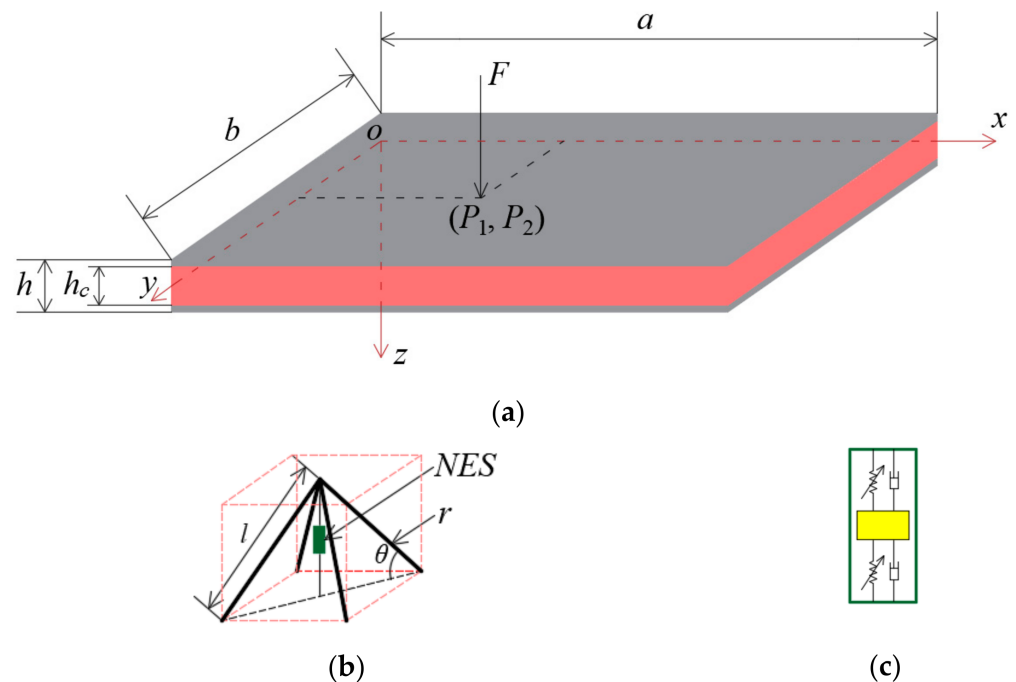

(a)

(b)

(c)

Figure 1. System model: (**a**) composite truss core sandwich plate excited by shock load; (**b**) the pyramidal truss core unit with the NES; and (**c**) the mechanical model of the NES.

Table 1. The symbolic representation of structural parameters.

Structural Parameters	Symbols
Plate length	*a*
Plate width	*b*
Plate height	*h*
Height of core layer	h_c
Rod length	*l*
Rod radius	*r*
Inclination angle	θ

Based on Allen's theory [39], the following assumptions are given as:

(1) The thickness of the truss core sandwich plate remains constant during deformation;
(2) Bending deformation only exists in the thin-face sheets, and shear one happens in the thick truss core of the plate;
(3) The deflections of the whole plate are continuous.

The thin-face sheets are made of carbon fiber composites, which are laid in five layers as $0/90/0/90/0$. The stress–strain relations for the composite material can be expressed as follows:

$$\begin{Bmatrix} \sigma_{xx} \\ \sigma_{yy} \\ \sigma_{xy} \end{Bmatrix} = \begin{Bmatrix} \overline{Q}_{11} & \overline{Q}_{12} & 0 \\ \overline{Q}_{21} & \overline{Q}_{22} & 0 \\ 0 & 0 & \overline{Q}_{66} \end{Bmatrix} \begin{Bmatrix} \varepsilon_{xx} \\ \varepsilon_{yy} \\ \gamma_{xy} \end{Bmatrix} \tag{1}$$

where the equivalent modulus $\overline{Q}_{ij}$ can be expressed as

$$\overline{Q}_{11} = Q_{11}\cos^4 \alpha + 2(Q_{12} + 2Q_{66})\sin^2 \alpha \cos^2 \alpha + Q_{22}\sin^4 \alpha \tag{2a}$$

$$\overline{Q}_{12} = (Q_{11} + Q_{22} - 4Q_{66})\sin^2 \alpha \cos^2 \alpha + Q_{12}(\sin^4 \alpha + \cos^4 \alpha) \tag{2b}$$

$$\overline{Q}_{22} = Q_{11}\sin^4 \alpha + 2(Q_{12} + 2Q_{66})\sin^2 \alpha \cos^2 \alpha + Q_{22}\cos^4 \alpha \tag{2c}$$

$$\overline{Q}_{66} = (Q_{11} + Q_{22} - 2Q_{12} - 2Q_{66})\sin^2 \alpha \cos^2 \alpha + Q_{66}(\sin^4 \alpha + \cos^4 \alpha) \tag{2d}$$

Here, Q_{ij} is the elastic constants and α is the stacking angle of the face sheet.

The first-order shear deformation theory is applied here to express the displacement fields of the structure as

$$u(x, y, z, t) = z\Psi_x(x, y, t) \tag{3a}$$

$$v(x, y, z, t) = z\Psi_y(x, y, t) \tag{3b}$$

$$w(x, y, z, t) = w_0(x, y, t) \tag{3c}$$

where Ψ_x and Ψ_y are the rotations of the transverse normal about the y- and x-axes, respectively.

The strains associated with the displacement field can be expressed as

$$\varepsilon_{xx} = z\frac{\partial \Psi_x}{\partial x}, \ \varepsilon_{yy} = z\frac{\partial \Psi_y}{\partial y}, \ \varepsilon_{zz} = 0$$

$$\gamma_{xy} = z\left(\frac{\partial \Psi_x}{\partial y} + \frac{\partial \Psi_y}{\partial x}\right), \ \gamma_{xz} = \frac{\partial w_0}{\partial x} + \Psi_x, \ \gamma_{yz} = \frac{\partial w_0}{\partial y} + \Psi_y \tag{4}$$

Applying the Hamilton's principle, the motion equations of the sandwich plate coupled with five NESs can be derived as

$$D_{11}\frac{\partial^2 \Psi_x}{\partial x^2} + D_{12}\frac{\partial^2 \Psi_y}{\partial x \partial y} + D_{66}\left(\frac{\partial^2 \Psi_x}{\partial y^2} + \frac{\partial^2 \Psi_y}{\partial x \partial y}\right) - \kappa A_{55}\left(\frac{\partial w_0}{\partial x} + \Psi_x\right) = I_2\ddot{\Psi}_x \tag{5a}$$

$$D_{22}\frac{\partial^2 \Psi_y}{\partial y^2} + D_{12}\frac{\partial^2 \Psi_x}{\partial x \partial y} + D_{66}\left(\frac{\partial^2 \Psi_y}{\partial x^2} + \frac{\partial^2 \Psi_x}{\partial x \partial y}\right) - \kappa A_{44}\left(\frac{\partial w_0}{\partial y} + \Psi_y\right) = I_2\ddot{\Psi}_y \tag{5b}$$

$$\kappa A_{55}\left(\frac{\partial w^2_0}{\partial x^2} + \frac{\partial \Psi_x}{\partial x}\right) + \kappa A_{44}\left(\frac{\partial w^2_0}{\partial y^2} + \frac{\partial \Psi_y}{\partial y}\right) + F\delta(x - P_1, y - P_2) - \mu_0\dot{w}_0$$

$$+ \sum_{i=1}^{5}\left[K_i(w_{ni} - w_{pi})^3 + \mu_i(\dot{w}_{ni} - \dot{w}_{pi})\right]\delta(x - A_i, y - B_i) = I_0\ddot{w}_0 \tag{5c}$$

$$m_i\ddot{w}_{ni} + K_i(w_{ni} - w_{pi})^3 + \mu_i(\dot{w}_{ni} - \dot{w}_{pi}) = 0 (i = 1, 2, 3, 4, 5) \tag{5d}$$

where

$D_{ij} = D_{ij1} + D_{ij3}(i, j = 1, 2, 6)$, $D_{ij1} = \int_{-\frac{h}{2}}^{-\frac{h_c}{2}} \overline{Q}_{ij}z^2 dz$, $D_{ij3} = \int_{\frac{h_c}{2}}^{\frac{h}{2}} \overline{Q}_{ij}z^2 dz$, $A_{44} = \int_{-\frac{h_c}{2}}^{\frac{h_c}{2}} G_{23c}dz$, $A_{55} = \int_{-\frac{h_c}{2}}^{\frac{h_c}{2}} G_{13c}dz$, $I_i = \sum_{k=1}^{N}\int_{z_k}^{z_{k+1}} \rho^{(k)}(z)^i dz(i = 0, 2)$, $w_{pi} = w_0(A_i, B_i, t)$ $(i = 1, 2, 3, 4, 5)$; here, (A_i, B_i) represent the locations of five NESs in the plate. m_i, μ_i, K_i, and w_{ni} are the mass, damping, stiffness, and displacements of the five NESs, respectively. μ_0 is the damping of the sandwich plate. κ is the shear correction coefficient. A_{44} and A_{55}

are the extensional stiffness. D_{ij} is the bending stiffness. The rotational inertia terms in Equation (5) can be ignored for the small values.

In order to obtain the dimensionless dynamic equation, the following transformations are introduced:

$$
\overline{w}_0 = \frac{w_0}{h}, \ \overline{w}_{ni} = \frac{w_{ni}}{h}, \ \overline{\Psi}_x = \Psi_x, \ \overline{\Psi}_y = \Psi_y, \ \overline{x} = \frac{x}{a}, \ \overline{y} = \frac{y}{b}, \ \overline{F} = \frac{a^2 b^2}{E_1 h^4} F,
$$
$$
\overline{\mu} = \frac{ab}{h^2} \left(\frac{1}{\rho E_1}\right)^{\frac{1}{2}} \mu, \ \overline{t} = \frac{h}{ab} \left(\frac{E_1}{\rho}\right)^{\frac{1}{2}} t, \ \overline{\Omega} = \frac{ab}{h} \left(\frac{\rho}{E_1}\right)^{\frac{1}{2}} \Omega, \ \overline{A}_{ij} = \frac{(ab)^{\frac{1}{2}}}{E_1 h^2} A_{ij}, \tag{6}
$$
$$
\overline{D}_{ij} = \frac{(ab)^{\frac{1}{2}}}{E_1 h^4} D_{ij}, \ \overline{K} = \frac{a^2 b^2}{E_1 h} K, \ \overline{m} = \frac{1}{(ab)^{\frac{1}{2}} \rho} m, \ \overline{I}_0 = \frac{1}{(ab)^{\frac{i+1}{2}} \rho} I_0
$$

For convenience, the "-" on the dimensionless symbols are ignored. Substituting Equation (6) into Equation (5), the dimensionless dynamical equations of the system can be written as

$$
q_{11} \frac{\partial^2 \Psi_x}{\partial x^2} + q_{12} \frac{\partial^2 \Psi_y}{\partial x \partial y} + q_{13} \frac{\partial^2 \Psi_x}{\partial y^2} - q_{14} \frac{\partial w_0}{\partial x} - q_{15} \Psi_x = 0 \tag{7a}
$$

$$
q_{21} \frac{\partial^2 \Psi_y}{\partial y^2} + q_{22} \frac{\partial^2 \Psi_x}{\partial x \partial y} + q_{23} \frac{\partial^2 \Psi_y}{\partial x^2} - q_{24} \frac{\partial w_0}{\partial y} - q_{25} \Psi_y = 0 \tag{7b}
$$

$$
\ddot{w}_0 + \gamma_0 \dot{w}_0 - q_{31} \frac{\partial w^2_0}{\partial x^2} - q_{32} \frac{\partial \Psi_x}{\partial x} - q_{33} \frac{\partial w^2_0}{\partial y^2} - q_{34} \frac{\partial \Psi_y}{\partial y}
$$
$$
+ \sum_{i=1}^{5} \left[k_i \left(w_{pi} - w_{ni}\right)^3 + \gamma_i \left(\dot{w}_{pi} - \dot{w}_{ni}\right) \right] \delta(x - a_i, y - b_i) = \Gamma \delta(x - p_1, y - p_2) \tag{7c}
$$

$$
\varepsilon_i \ddot{w}_{ni} + k_i \left(w_{ni} - w_{pi}\right)^3 + \gamma_i \left(\dot{w}_{ni} - \dot{w}_{pi}\right) = 0 \ (i = 1, 2, 3, 4, 5) \tag{7d}
$$

where

$$
q_{11} = \frac{h^2}{a^2} D_{11}, \ q_{12} = \frac{h^2}{ab}(D_{12} + D_{66}), \ q_{13} = \frac{h^2}{b^2} D_{66}, \ q_{14} = \frac{\kappa h}{a} A_{55}, \ q_{15} = \kappa A_{55}, \ q_{21} = \frac{h^2}{b^2} D_{22},
$$
$$
q_{22} = \frac{h^2}{ab}(D_{12} + D_{66}), \ q_{23} = \frac{h^2}{a^2} D_{66}, \ q_{24} = \frac{\kappa h}{b} A_{44}, \ q_{25} = \kappa A_{44}, \ q_{31} = \frac{\kappa b A_{55}}{a I_0}, \ q_{32} = \frac{\kappa b A_{55}}{h I_0}, \ q_{33} = \frac{\kappa a A_{44}}{b I_0},
$$
$$
q_{34} = \frac{\kappa a A_{44}}{h I_0}, \ \gamma_0 = \frac{h \mu_0}{(ab)^{\frac{1}{2}} I_0}, \ \gamma_i = \frac{h \mu_i}{(ab)^{\frac{1}{2}} I_0}, \ k_i = \frac{h K_i}{(ab)^{\frac{1}{2}} I_0}, \ \Gamma = \frac{h F}{(ab)^{\frac{1}{2}} I_0}, \ \varepsilon_i = \frac{m_i}{I_0}, \ p_1 = \frac{P_1}{a},
$$
$$
p_2 = \frac{P_2}{b}, \ a_i = \frac{A_i}{a}, \ b_i = \frac{B_i}{b}.
$$

Based on the simply supported boundary conditions of the composite truss core sandwich plate, Ψ_x, Ψ_y, and w_0 can be expressed as

$$
\Psi_x = \sum_{n=1}^{\infty} \sum_{m=1}^{\infty} 2x_{mn}(t) \cos m\pi x \sin n\pi y \tag{8a}
$$

$$
\Psi_y = \sum_{n=1}^{\infty} \sum_{m=1}^{\infty} 2y_{mn}(t) \sin m\pi x \cos n\pi y \tag{8b}
$$

$$
w_0 = \sum_{n=1}^{\infty} \sum_{m=1}^{\infty} 2w_{mn}(t) \sin m\pi x \sin n\pi y \tag{8c}
$$

Since the harmful vibration of low frequency is the main cause of structural damage, here, we focus on the response absorption of the first three vibration modes for the plate. Using the Galerkin method, the dimensionless dynamic equations of the motion for the coupled system can be obtained as follows:

$$
\ddot{w}_1 + \gamma_0 \dot{w}_1 + \omega_1^2 w_1 + \sum_{i=1}^{5} k_i [w_1 q_1(a_i, b_i) + w_2 q_2(a_i, b_i) + w_3 q_3(a_i, b_i) - w_{ni}]^3 q_1(a_i, b_i)
$$
$$
+ \sum_{i=1}^{5} \gamma_i \left[\dot{w}_1 q_1(a_i, b_i) + \dot{w}_2 q_2(a_i, b_i) + \dot{w}_3 q_3(a_i, b_i) - \dot{w}_{ni}\right] q_1(a_i, b_i) = \Gamma q_1(p_1, p_2) \tag{9a}
$$

$$\ddot{w}_2 + \gamma_0 \dot{w}_2 + \omega_2^2 w_2 + \sum_{i=1}^{5} k_i [w_1 q_1(a_i, b_i) + w_2 q_2(a_i, b_i) + w_3 q_3(a_i, b_i) - w_{ni}]^3 q_2(a_i, b_i)$$

$$+ \sum_{i=1}^{5} \gamma_i [\dot{w}_1 q_1(a_i, b_i) + \dot{w}_2 q_2(a_i, b_i) + \dot{w}_3 q_3(a_i, b_i) - \dot{w}_{ni}] q_2(a_i, b_i) = \Gamma q_2(p_1, p_2) \tag{9b}$$

$$\ddot{w}_3 + \gamma_0 \dot{w}_3 + \omega_3^2 w_3 + \sum_{i=1}^{5} k_i [w_1 q_1(a_i, b_i) + w_2 q_2(a_i, b_i) + w_3 q_3(a_i, b_i) - w_{ni}]^3 q_3(a_i, b_i)$$

$$+ \sum_{i=1}^{5} \gamma_i [\dot{w}_1 q_1(a_i, b_i) + \dot{w}_2 q_2(a_i, b_i) + \dot{w}_3 q_3(a_i, b_i) - \dot{w}_{ni}] q_3(a_i, b_i) = \Gamma q_3(p_1, p_2) \tag{9c}$$

$$\varepsilon_i \ddot{w}_{ni} + k_i [w_{ni} - w_1 q_1(a_i, b_i) - w_2 q_2(a_i, b_i) - w_3 q_3(a_i, b_i)]^3$$

$$+ \gamma_i [\dot{w}_{ni} - \dot{w}_1 q_1(a_i, b_i) - \dot{w}_2 q_2(a_i, b_i) - \dot{w}_3 q_3(a_i, b_i)] = 0 (i = 1, 2, 3, 4, 5) \tag{9d}$$

where ω_1, ω_2, and ω_3 are the first three natural frequencies of the sandwich plate. $q_1(x, y)$, $q_2(x, y)$, and $q_3(x, y)$ are the components acting on the first three modes.

3. Overall Performances for the Five NESs

Numerical simulation methods are applied here to analyze the overall performances of the five NESs absorber. To be clear, the units of the sandwich plate are numbered sequentially as shown in Figure 2. The locations of the five NESs are circled in red in Figure 2, where N_1 corresponds to the coordinate point (0.5, 0.5), and N_2, N_3, N_4 and N_5 are symmetrically distributed around. In the following study, let N_2, N_3, N_4, and N_5 change synchronously to keep their symmetry of the center, and the position of the four NESs can be adjusted by changing the position of the N_2 coordinate (a_2, b_2).
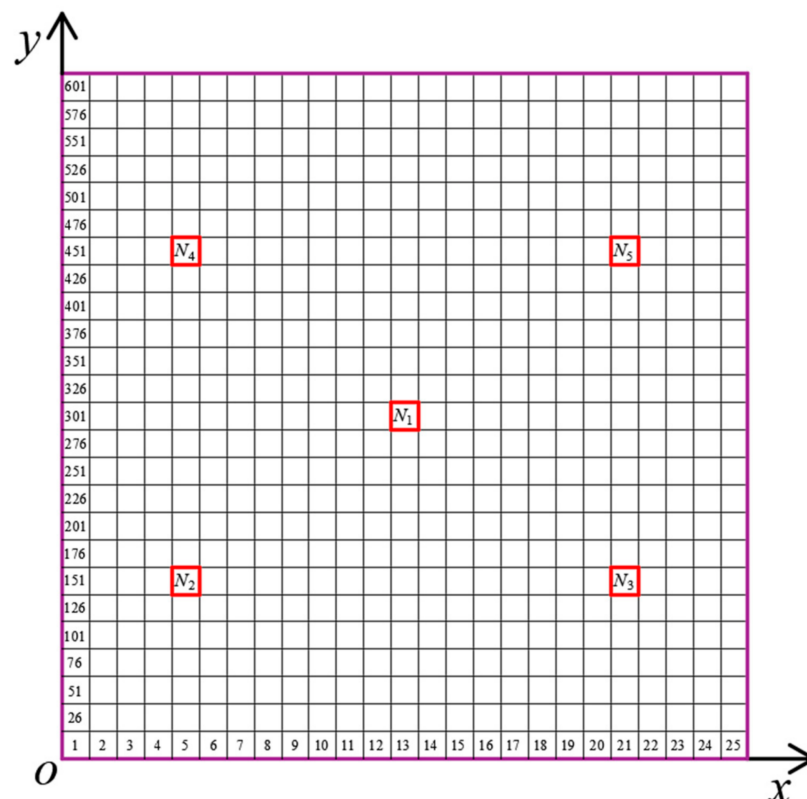

Figure 2. Units in two-dimensional coordinate system.

The geometry and material property parameters of the sandwich plate used in this paper are shown in Table 2. In addition, the thickness of each lamina is 0.12 mm.

Table 2. Geometry and material property parameters of the sandwich plate.

Items	Values
Density	$\rho = 1570 \text{ kg/m}^3$
Poisson's ratios	$\nu_{12} = 0.25$ $\nu_{13} = 0.25$ $\nu_{23} = 0.38$
Elastic moduli	$E_1 = 1.32 \times 10^5 \text{ MPa}$ $E_2 = 1.03 \times 10^4 \text{ MPa}$ $E_3 = 1.03 \times 10^4 \text{ MPa}$
Shear moduli	$G_{12} = 6.5 \times 10^3 \text{ MPa} \ G_{13} = 6.5 \times 10^3 \text{ MPa}$ $G_{23} = 3.91 \times 10^3 \text{ MPa}$
Plate length	$a = 1 \text{ m}$
Plate width	$b = 1 \text{ m}$
Rod length	$l = 0.04 \text{ m}$
Inclination angle	$\theta = \pi/4$
Rod radius	$r = 1 \times 10^{-3} \text{ m}$

The shock load Γ is in the form of a half-sine pulse as

$$\Gamma = \begin{cases} f \sin(2\pi t/T) & 0 \leq t \leq T/2 \\ 0 & t > T/2 \end{cases} (T = 0.4/\pi) \tag{10}$$

The equivalent density of the truss core [39,40] is expressed as

$$\rho_c = \frac{2\pi\rho}{\cos^2\theta \sin\theta} \left(\frac{r}{l}\right)^2 \tag{11}$$

The shear modulus of the truss core [39,40] are written as

$$G_{13c} = G_{23c} = \pi \sin\theta \left(\frac{r}{l}\right)^2 E_1 \tag{12}$$

3.1. Determination of the Optimal Positions of Five NESs

The optimal positions of vibration suppression for the five NESs are discussed firstly. Let the parameters of the five NESs be equal, which include stiffness, damping, and mass. Moreover, the arbitrary dimensionless parameters are set to $\varepsilon_i = 0.02$, $\gamma_i = 0.05$, and $k_i = 800$. The following study is done in three steps. In the first one, suppose the shock force acts on the point $(p_1 = 0.35, p_2 = 0.35)$ and its amplitudes are $f = 1, f = 3,$ and $f = 5$, respectively. Based on the numbering sequence in Figure 2, N_2 is placed in the different number units in sequence from small to large.

The energy dissipation ratio is introduced, and dynamic equations of the system are solved by the Runge Kutta method to analyze the overall efficiency of the five NESs with different distributions [32]. The energy dissipation ratio is calculated using the following expression:

$$\eta = \frac{\sum\limits_{i=1}^{5} \gamma_i \int_0^t \left[\dot{w}_1 q_1(a_i, b_i) + \dot{w}_2 q_2(a_i, b_i) + \dot{w}_3 q_3(a_i, b_i) - \dot{w}_{ni}\right]^2 d\tau}{\int_0^T \Gamma\left[\dot{w}_1 q_1(p_1, p_2) + \dot{w}_2 q_2(p_1, p_2) + \dot{w}_3 q_3(p_1, p_2)\right] dt} \tag{13}$$

Figure 3 shows the energy dissipation ratios of five NESs at different positions, where different colors indicate the energy dissipation ratios of the NESs. It can be found that there are optimal energy dissipation areas for the five NESs. No matter how big the amplitudes of the shock force, the optimal area distributions for vibration-suppression are similar to each other. Therefore, the optimal vibration-suppression area of the five NESs can be selected as

a rough range, which is surrounded by the black boxes in Figure 3. The corner coordinates of these black boxes are marked as S_1, S_2, S_3, and S_4, which are

$$S_1 = \{(0.2, 0.2), (0.4, 0.2), (0.2, 0.4), (0.4, 0.4)\},$$

$$S_2 = \{(0.6, 0.2), (0.8, 0.2), (0.6, 0.4), (0.8, 0.4)\},$$

$$S_3 = \{(0.2, 0.6), (0.4, 0.6), (0.2, 0.8), (0.4, 0.8)\},$$

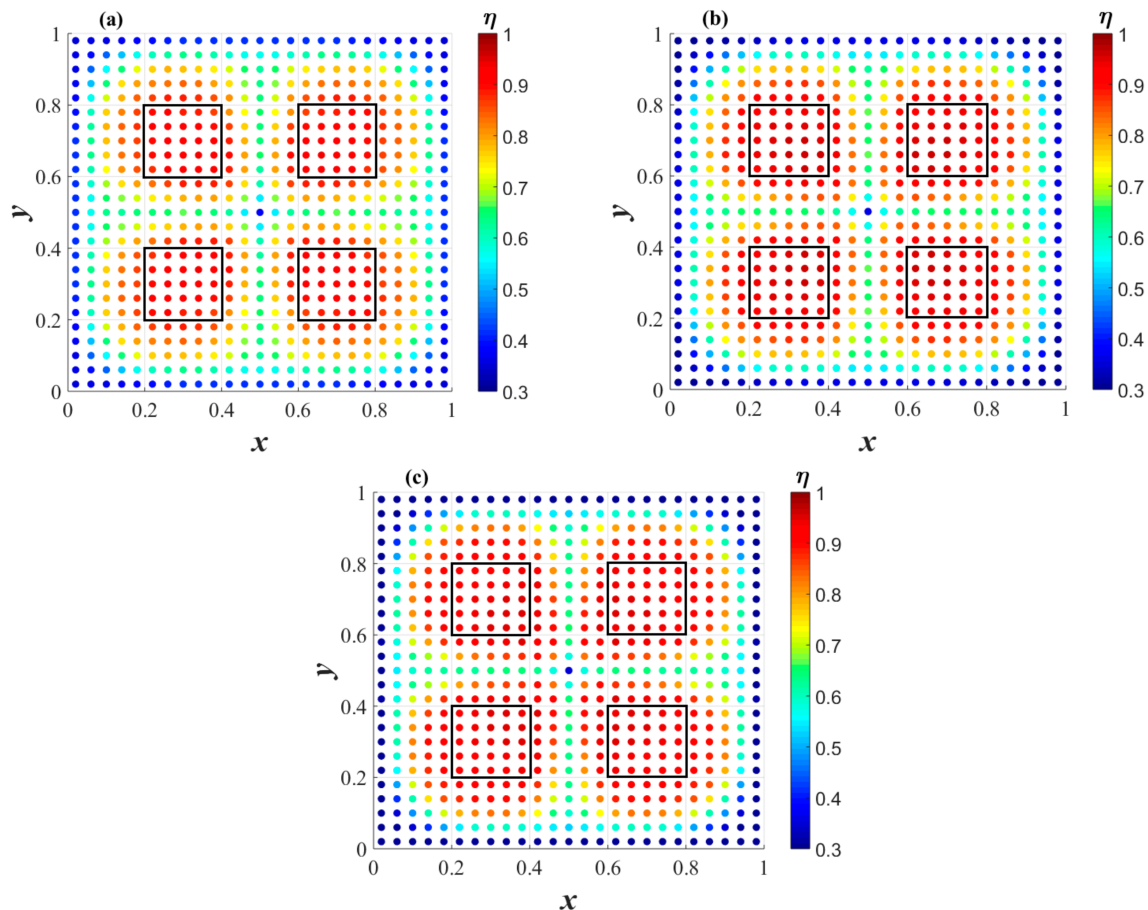$$S_4 = \{(0.6, 0.6), (0.8, 0.6), (0.6, 0.8), (0.8, 0.8)\}.$$

Figure 3. Energy dissipation ratios of five NESs at different positions under different excitation amplitudes: (**a**) $f = 1$; (**b**) $f = 3$; and (**c**) $f = 5$.

In the second step, chose two different locations of the five NESs as an example, where one is in the optimal position range as $(a_2 = 0.3, b_2 = 0.3)$ and the other is out of this range as $(a_2 = 0.18, b_2 = 0.18)$. Meanwhile, keep the dimensionless shock amplitude f as 1, and then the transient responses of the sandwich plate without and with the five NESs in two different positions are shown in Figure 4, in which the vertical coordinate w is the sum amplitudes of the first three modes. In order to facilitate comparison, the time required for the system to return to the static state after being shocked is defined as the effective suppression time. It is easy to see that the effective suppression time of $(a_2 = 0.3, b_2 = 0.3)$ is obviously less than that of $(a_2 = 0.18, b_2 = 0.18)$. Therefore, the layout for the five NESs in Figure 4a is much better than that in Figure 4b, and the optimal position can make the five NESs work efficiently.
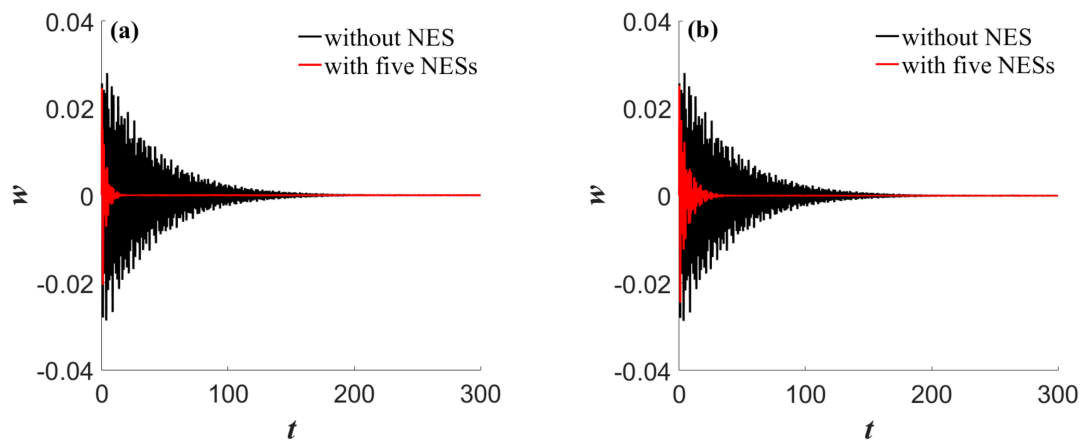
Figure 4. Comparison of vibration-reduction performance of five NESs under different locations: (**a**) the responses when $(a_2 = 0.3, b_2 = 0.3)$; (**b**) the responses when $(a_2 = 0.18, b_2 = 0.18)$.

In the third step, keep the shock amplitude $f = 5$ and change the location of the shock. Figure 5 shows the energy dissipation ratios of the five NESs with the shock force on $(p_1 = 0.5, p_2 = 0.5)$ and $(p_1 = 0.5, p_2 = 0.3)$. From Figure 5a,b and Figure 3c, it is found that the optimal position distribution of the five NESs will change with the loading position. Thus, set the shock force at the position $(p_1 = 0.35, p_2 = 0.35)$ and the five NESs at $(a_2 = 0.3, b_2 = 0.38)$ for the following research.
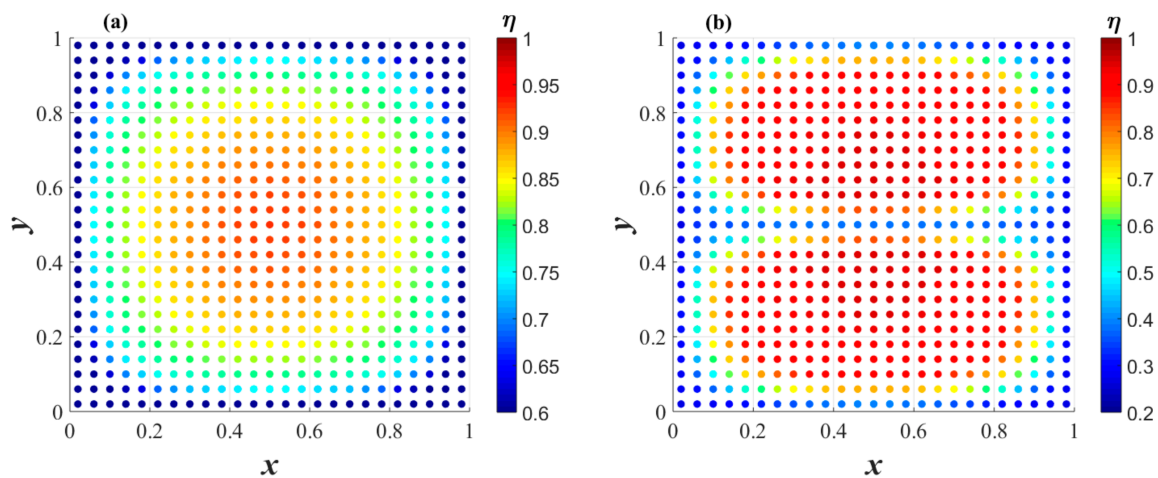
Figure 5. The energy dissipation ratios of five NESs at different positions when $f = 5$: (**a**) $(p_1 = 0.5, p_2 = 0.5)$; (**b**) $(p_1 = 0.5, p_2 = 0.3)$.

3.2. Research on Transient Responses Based on the Optimal Position

The five NESs are placed inside the sandwich plate, and the relative motion between each substructure and the mid-plane of the sandwich plate should also be taken into account. $w_{ri}(i = 1, 2, 3, 4, 5)$ are the relative displacements between the center of the mass block and the mid-plane of the sandwich plate, which are used to study whether the five NESs will collide with the sandwich plate. In the case that the volumes of the internal five NESs are all ignored, by the position of the coordinate system and the parameters of the structure, the effective relative motion range in which the five NESs will not collide with the face sheets of sandwich plate is $-h_c/2h < w_{ri} < h_c/2h$. Here, two different amplitudes of the load are considered, including $f = 5$ and $f = 10$. The relative displacements between the NESs and the sandwich plate are shown in Figures 6 and 7, respectively. With the increase of force, the duration of relative motion between the sandwich plate and the NESs is longer. Obviously, due to different positions, the maximum relative displacement between each substructure and the sandwich plate is different, but they are all within a reasonable range.
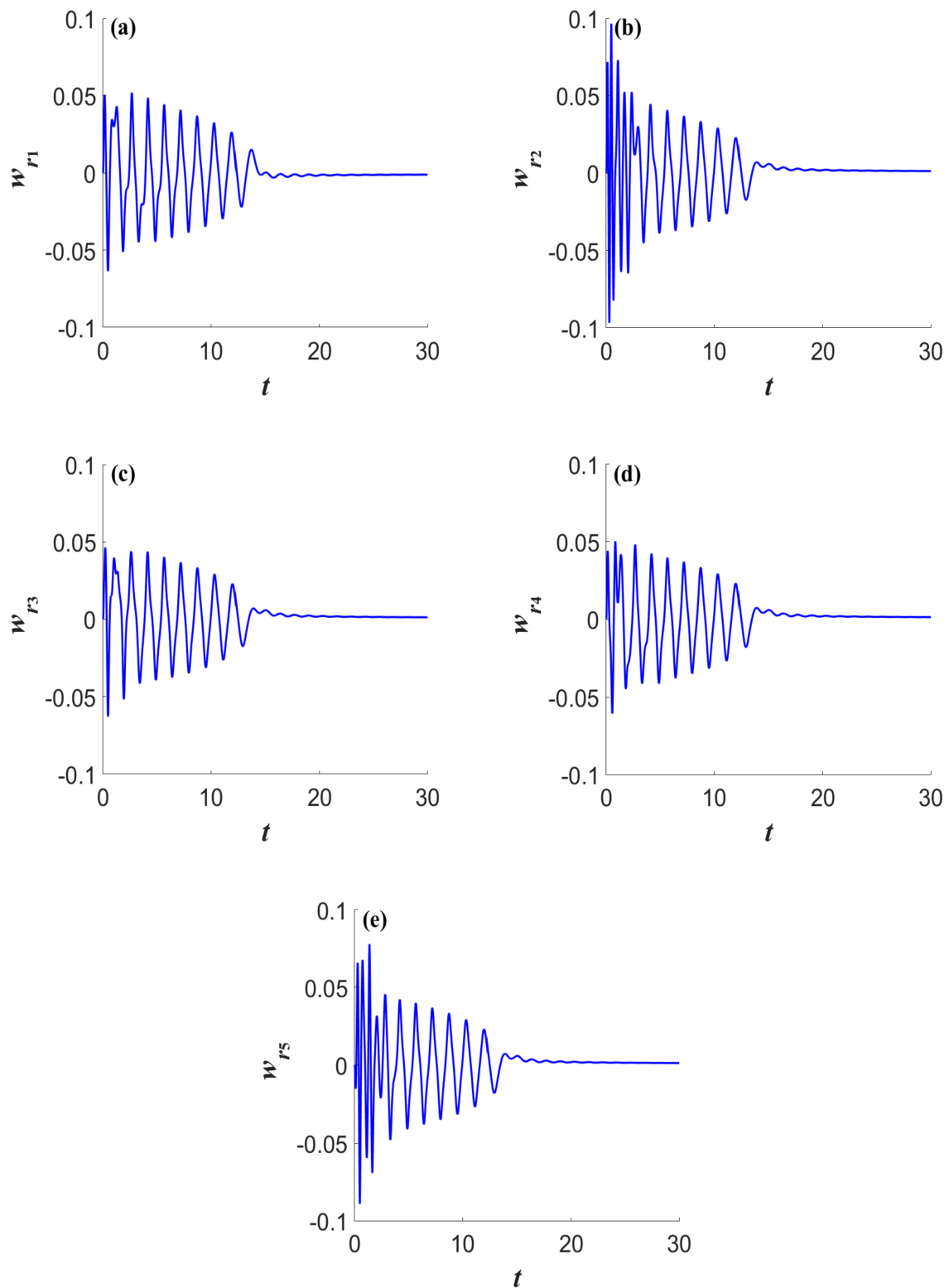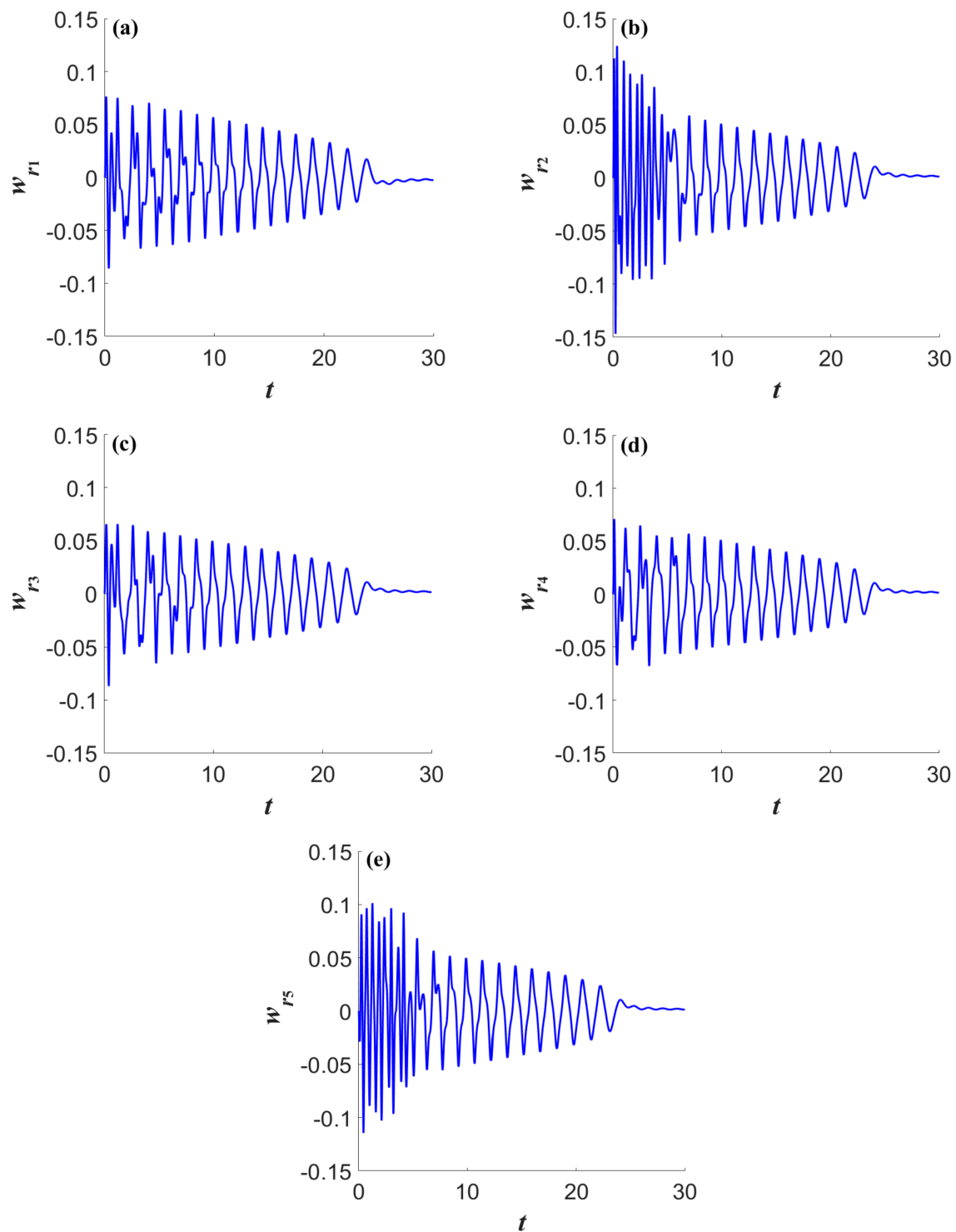
Figure 6. The relative motion between the plate and each substructure of five NESs when $f = 5$: (**a**) the relative motion between the plate and the N_1; (**b**) the relative motion between the plate and the N_2; (**c**) the relative motion between the plate and the N_3; (**d**) the relative motion between the plate and the N_4; and (**e**) the relative motion between the plate and the N_5.

Figure 7. The relative motion between the plate and each substructure of five NESs when $f = 10$: (**a**) the relative motion between the plate and the N_1; (**b**) the relative motion between the plate and the N_2; (**c**) the relative motion between the plate and the N_3; (**d**) the relative motion between the plate and the N_4; and (**e**) the relative motion between the plate and the N_5.

w_1, w_2, and w_3, respectively, represent the response amplitudes of the first three modes of the sandwich plate. Figures 8–10, respectively, show the waveforms of the first three transient responses for the sandwich plate without and with five NESs under different excitation amplitudes. It can be clearly found that no matter how large the excitation amplitude is, the five NESs in the optimal position always has a good vibration-

reduction effect on the first three modes of the plate. Furthermore, under the same excitation amplitude, the five NESs in the optimal position have different vibration-reduction effects on the first three modes.
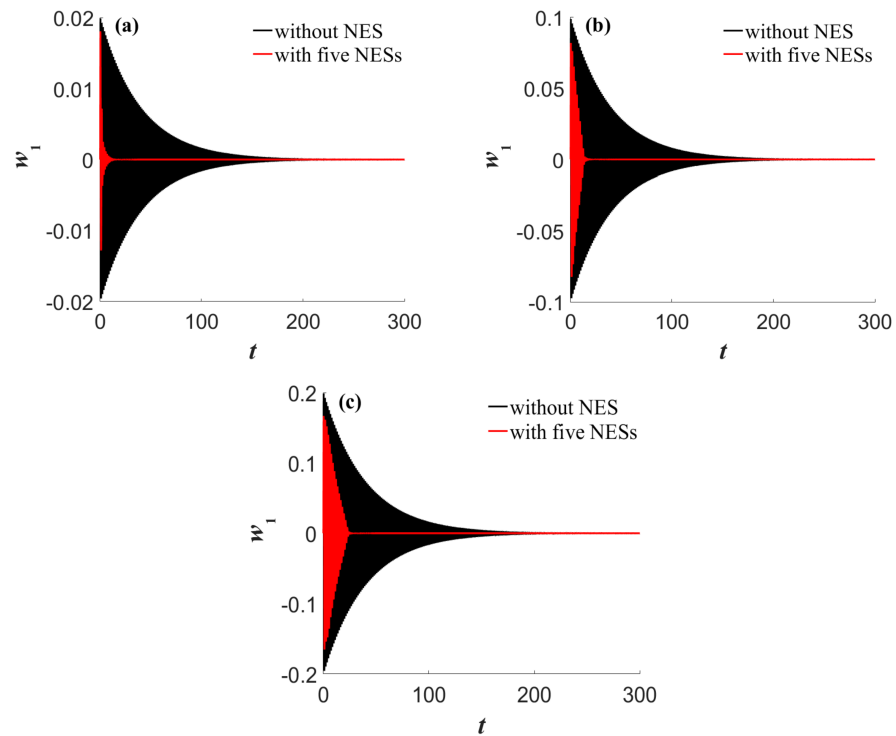

Figure 8. The first-order transient response of sandwich plate under different excitation amplitudes: (**a**) $f = 1$; (**b**) $f = 5$; and (**c**) $f = 10$.
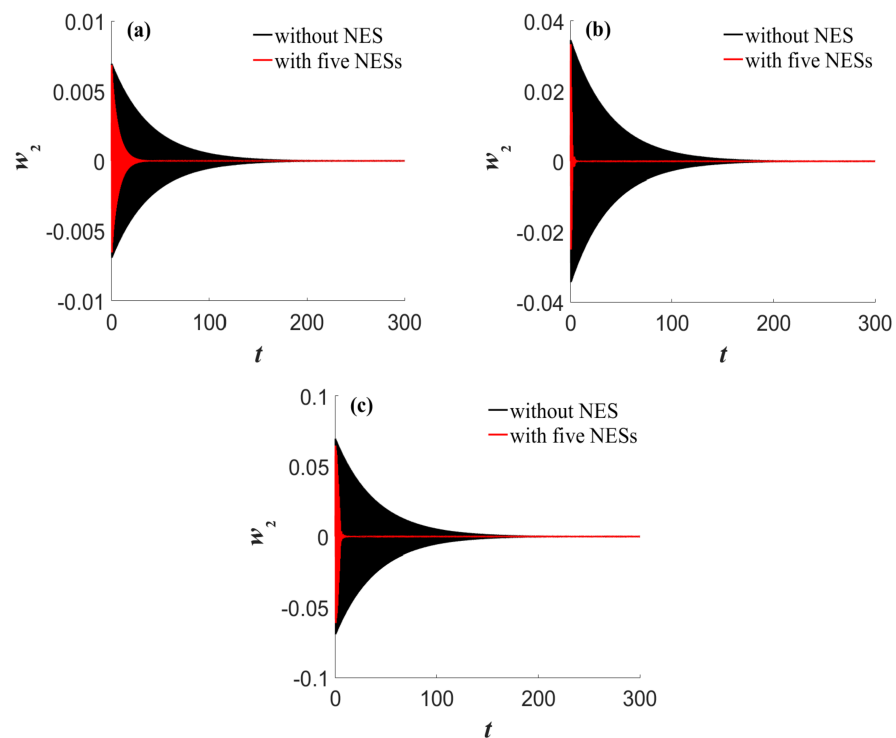

Figure 9. The second-order transient response of sandwich plate under different excitation amplitudes: (**a**) $f = 1$; (**b**) $f = 5$; and (**c**) $f = 10$.
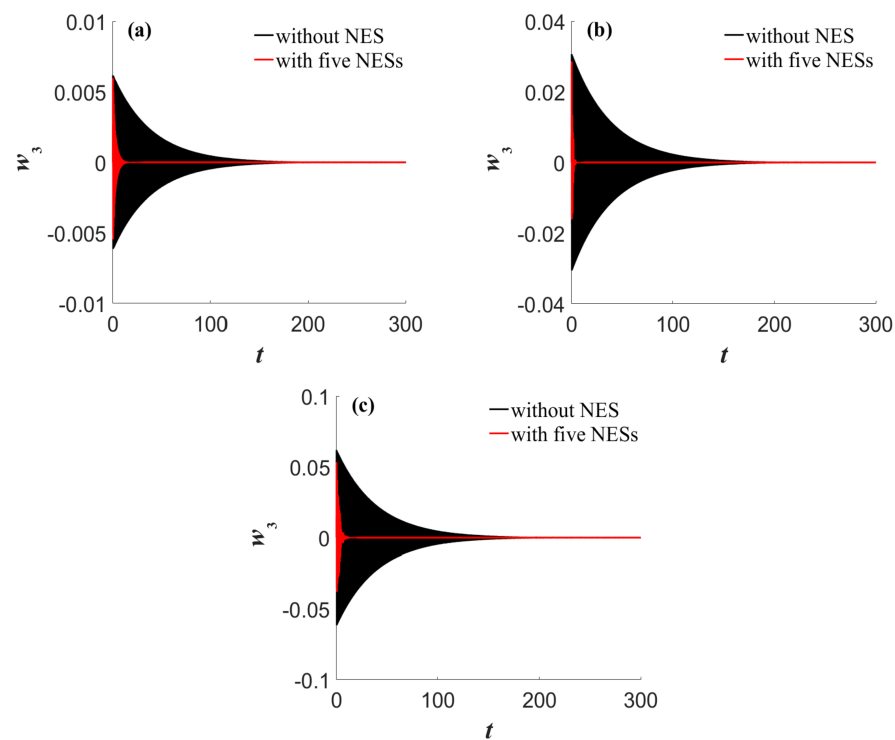
Figure 10. The third-order transient response of sandwich plate under different excitation. Amplitudes: (**a**) $f = 1$; (**b**) $f = 5$; and (**c**) $f = 10$.

3.3. Comparison of Single NES and Five NESs

In this part, the performances of the five NESs in the optimal vibration-suppression area are compared with that of a single NES. Firstly, the optimal suppression positions for the single NES are obtained by successively locating it in the different units of the sandwich plate, and the energy dissipation ratios of the single NES are obtained with different excitation amplitudes in Figure 11.

Unlike the five NESs, some optimal positions of a single NES will change with the excitation amplitude, but some optimal positions that do not change with the excitation amplitude can still be identified, such as the ones surrounded by black boxes in Figure 11, which are located in

$$S\prime_1 = \{(0.28,\ 0.28),\ (0.40,\ 0.28),\ (0.28,\ 0.40),\ (0.40,\ 0.40)\};$$

$$S\prime_2 = \{(0.60,\ 0.60),\ (0.72,\ 0.60),\ (0.60,\ 0.72),\ (0.72,\ 0.72)\}.$$

For a better comparison, choose a position within the optimal position range of a single NES for the following analysis, which is selected here as (0.34, 0.34).

Assuming that the nonlinear absorbers are all in the optimal position, Figure 12 gives the energy dissipation ratios of the single and five NESs with the same shock. ε_t is the sum of the mass coefficients of the five substructures, and the total mass of the absorber can be changed by ε_t. Through the trajectories of different color curves, it can see that the same trend of vibration reduction exists for the five NESs, that is, no matter how the total mass changes, the efficiency of the five NESs gradually decreases when the excitation amplitude increases to a certain threshold. The efficiency of the five NESs can be improved a lot by increasing the total mass of the five NESs until ε_t equals 0.06. Moreover, the vibration-absorption effect of five NESs is better than that of single NES at the same mass. It still can dominate in the most of the amplitude range when ε_t reduces to 0.04. Even the ε_t decreases to 0.02, there also exists an small advantage area for the five NESs from $f = 0.1$ to $f = 1.3$.
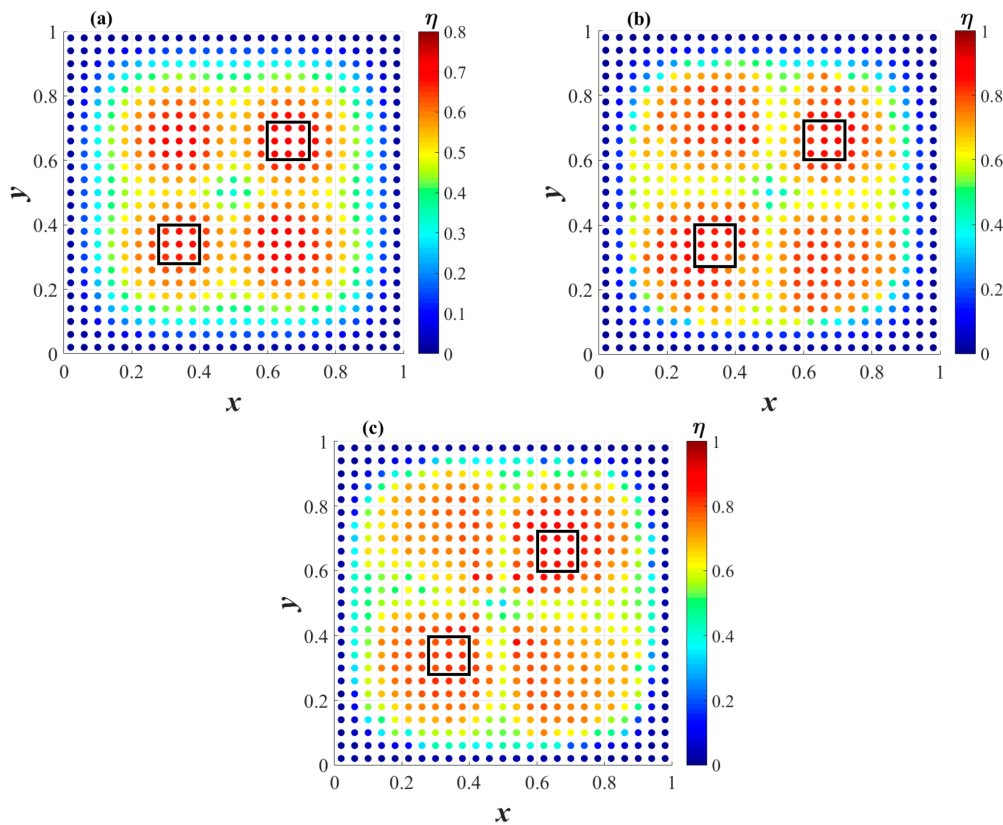
Figure 11. The energy dissipation ratios of single NES at different positions under different excitation amplitudes: (**a**) $f = 1$; (**b**) $f = 3$; and (**c**) $f = 5$.
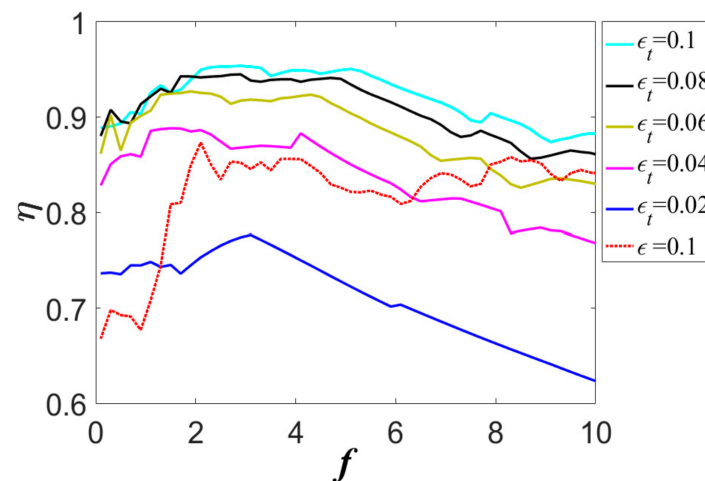

Figure 12. The energy dissipation ratios of single NES and five NESs with shock amplitude (the solid line represents the five NESs, the dashed line represents the single NES).

3.4. The Effect of Five NESs Parameters

Through the previous analysis, it can be found that the five NESs considering the optimal positions have great advantages in vibration reduction. In this part, the influence of relevant parameters on the vibration-reduction performance of the five NESs is analyzed. ε_t is chosen as 0.04 for the following parameter optimization based on Figure 12. The amplitude of the shock force is set as $f = 5$, and the other parameters of the five NESs keep the same as in Figure 3. Figure 13 shows the effect of the nonlinear stiffness of the NESs on the vibration absorption, which indicts that with the increase of nonlinear stiffness, the efficiency of the five NESs increases firstly and decreases later. The effect of the damping of

the five NESs on the vibration absorption is consistent with that of the stiffness, as shown in Figure 14.
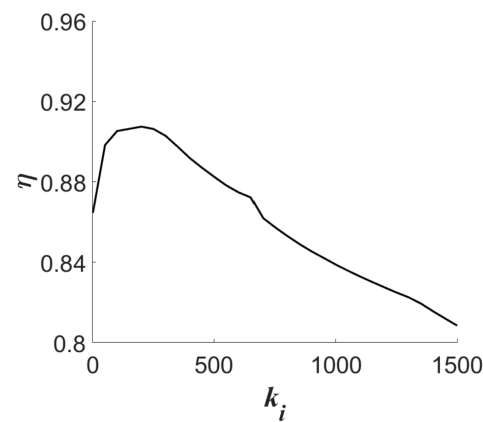

Figure 13. The variation of efficiency of the five NESs with nonlinear stiffness.
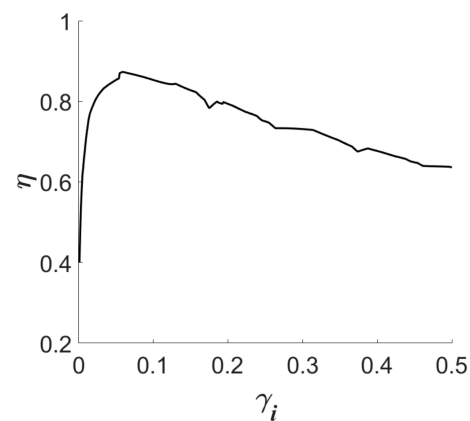

Figure 14. The variation of efficiency of the five NESs with damping.

The discrepancies of the center one and the other four NESs are also considered. First, change the mass of the five substructures. Let the mass coefficient of N_1 be ε_1; the mass coefficients of the other four NESs (N_n, n = 2, 3, 4, 5) are the same as $(\varepsilon_t - \varepsilon_1)/4$. Choose the ε_t as 0.02, 0.04, 0.06, 0.08 and 0.1, respectively. The effects of mass distribution on the efficiency of the NESs system are shown in Figure 15. It can be found that the overall efficiency of the five NESs is better with smaller N_1 and larger N_n (n = 2, 3, 4, and 5).
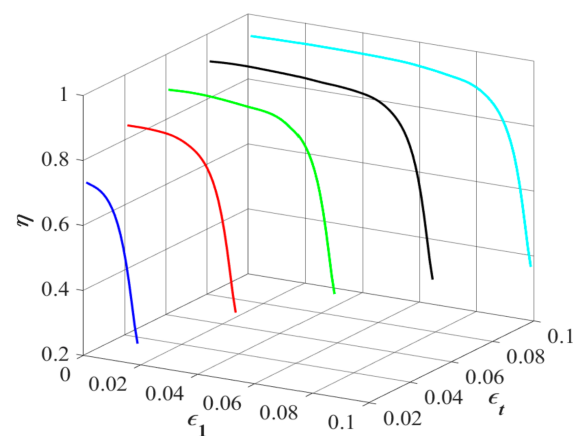

Figure 15. The variation of efficiency of the five NESs with the mass coefficient of N_1.

Moreover, the influences of the damping and stiffness of N_1 on the efficiency of the five NESs are also discussed. k_t and γ_t are the sum of stiffness and sum of damping of the five substructures, respectively. The stiffness and damping of N_1 are expressed as k_1 and γ_1, and the same parameters of the other four NESs are written as $(k_t - k_1)/4$ and $(\gamma_t - \gamma_1)/4$, respectively. The total stiffness and damping of the five NESs are chosen as 300, 600, 900, 1200, and 1500, and 0.1, 0.2, 0.3, 0.4, and 0.5, respectively. It is found that the effects of stiffness and damping of N_1 on the overall efficiency are similar; they increase at first and then decrease with the increased ratios of damping and stiffness of N_1, which are shown in Figures 16 and 17, respectively.
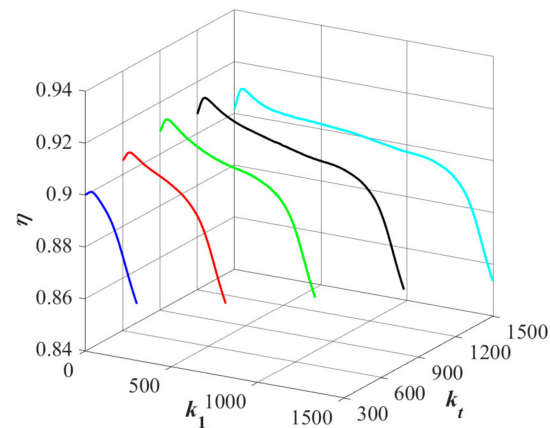

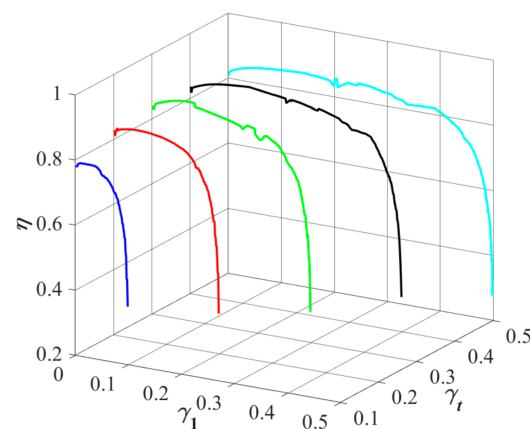**Figure 16.** The variation of efficiency of the five NESs with the stiffness of N_1.

Figure 17. The variation of efficiency of the five NESs with the damping of N_1.

Finally, the distribution methods of the five NESs are also analyzed. Name the aforementioned layout way (N_1 in the center and the other four around) as case 1. Then, place N_1 in the optimal position of a single NES (0.34, 0.34), and the other four are laid out like case 2 in Figure 18. By changing the coordinate (a_2, b_2) as before, the five NESs are distributed at all positions in the sandwich plate. The energy dissipation ratios of the five NESs in case 2 are obtained in Figure 19a–c, respectively, when $f = 1$, $f = 3$, and $f = 5$. Obviously, the coordinate (0.3, 0.38) in the black box is also in the range of the best vibration-suppression position, as in case 1. Therefore, keep N_2 in (0.3, 0.38) in both two cases; then, the vibration-absorption effect of the five NESs with excitation amplitude is shown in Figure 20, which indicates that the varied position of N_1 can improve the performance of the five NESs, such as $f = 0.1\sim5.9$. In addition, the reasonable design of the parameters (mass, stiffness, and damping) of the absorbers in case 2 can effectively improve the overall vibration-reduction efficiency of the five NESs, which is the same as that of case 1, so it will not be described here.
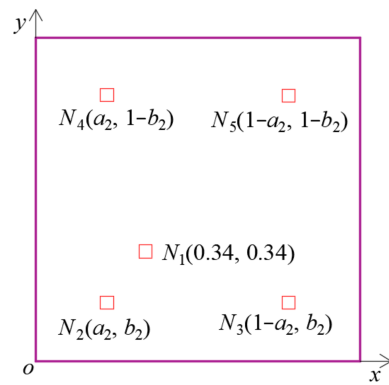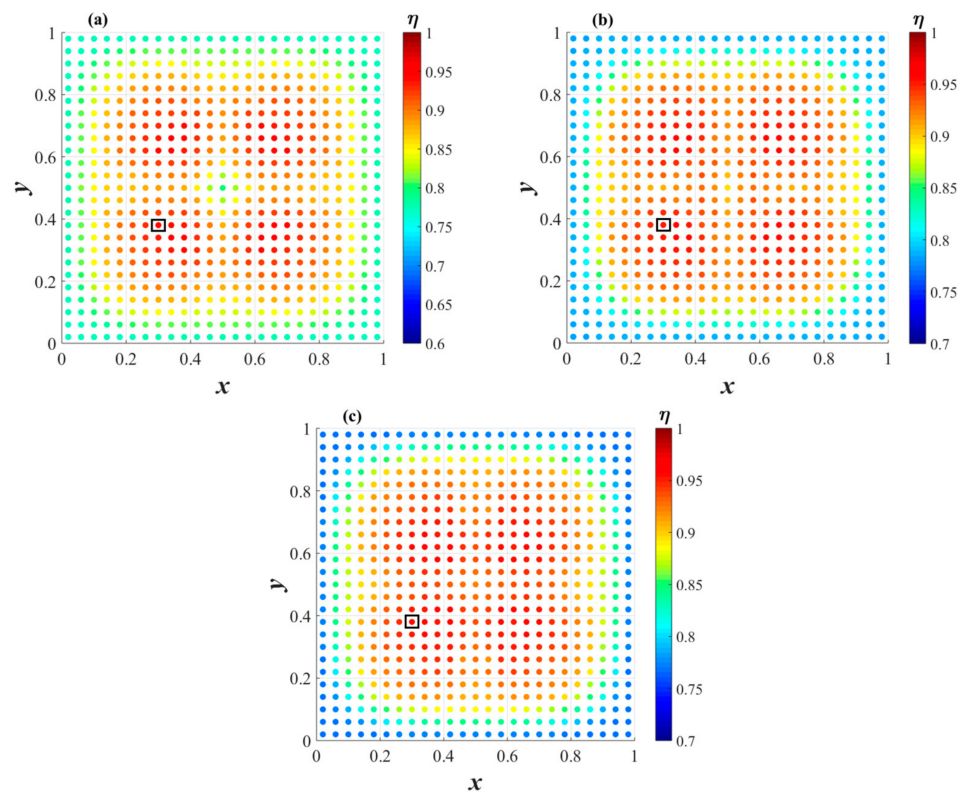
Figure 18. The layout case 2 of the five NESs.

Figure 19. The energy dissipation ratios of the five NESs at different positions under different excitation amplitudes (case 2): (**a**) $f = 1$; (**b**) $f = 3$; and (**c**) $f = 5$.
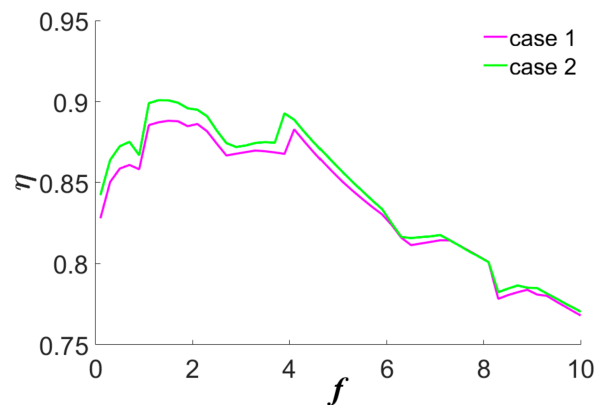

Figure 20. Comparison of two layout cases under different excitation amplitudes.

4. Conclusions

In this paper, the vibration-absorption effects of the internal five NESs, considering the optimal locations on the composite truss core sandwich plate, are investigated with shock excitations. The nonlinear dynamical equations of motion for the coupled system are built by the first-order shear deformation theory and the Galerkin method, and then the vibration-control performances of the five NESs are analyzed by numerical methods.

Firstly, the results find that the position distribution of both the five NESs and shock excitation have a great influence on the vibration suppression, but the excitation amplitude has little effect on the optimal area for the five NESs. Then, based on the optimal energy absorption area, the feasibility of the scheme and the action of five NESs on the first three modes of the sandwich plate are discussed. The performances of the single and the five NESs in the optimal position are compared, and the five NESs present much better suppression than the single one. It is found that for a larger range of excitation amplitudes, the best suppression mass of the five NESs can decrease 60% compared with the single NES. The smaller the excitation amplitude, the more obvious the quality advantage of the five NESs. Therefore, the reasonable distribution of multi NESs in multi-dimensional space has high values of small total mass and high efficiency in vibration-control fields.

In addition, the influence of the parameters on the efficiency of the five NESs is also studied to further improve the vibration suppression. Finally, two different layout ways are selected to discuss the effects of the position N_1 on the characters of the five NESs, which show that the varied position of N_1 can improve the performance of the five NESs.

Author Contributions: Conceptualization, W.Z. (Wei Zhang); methodology, X.G. and W.Z. (Weixing Zhang); validation, Z.L.; supervision, J.C.; and writing—W.Z. (Weixing Zhang). All authors have read and agreed to the published version of the manuscript.

Institutional Review Board Statement: Not applicable.

Informed Consent Statement: Not applicable.

Data Availability Statement: Not applicable.

Conflicts of Interest: The authors declare no conflict of interest.

References

1. Li, X.D.; Xiong, J.; Ma, L.; Wu, L.Z.; Yan, X.Q. Effect of vacuum thermal cycling on the compression and shear performance of composite sandwich structures containing pyramidal truss cores. *Compos. Sci. Technol.* **2018**, *158*, 67–78. [CrossRef]
2. Qi, G.; Ma, L.; Wang, S.Y. Modeling and reliability of insert in composite pyramidal lattice truss core. *Compos. Struct.* **2019**, *221*, 110888. [CrossRef]
3. Shen, C.; Xin, F.X.; Lu, T.J. Theoretical model for sound transmission through finite sandwich structures with corrugated core. *Int. J. Non-Linear Mech.* **2012**, *47*, 1066–1072. [CrossRef]
4. Zhang, X.Y.; Zhou, H.; Shi, W.H.; Zeng, F.M.; Zeng, H.Z. Vibration tests of 3D printed satellite structure made of lattice sandwich panels. *AIAA J.* **2018**, *10*, 4213–4217. [CrossRef]
5. Zhang, W.; Wu, Q.L.; Yao, M.H.; Dowell, E.H. Anaysis on global and chaotic dynamics of nonlinear wave equations for truss core sandwich plate. *Nonlinear Dyn.* **2018**, *94*, 21–37. [CrossRef]
6. Wang, D.W.; Ma, L.; Wang, X.T.; Wen, Z.H.; Glorieux, C. Sound transmission loss of laminated composite sandwich structures with pyramidal truss cores. *Compos. Struct.* **2019**, *220*, 19–30. [CrossRef]
7. Zangana, S.; Epaarachchi, J.; Ferdous, W.; Leng, J.S.; Schubel, P. Behaviour of continuous fibre composite sandwich core under low-velocity impact. *Thin-Walled Struct.* **2021**, *158*, 107157. [CrossRef]
8. Lou, J.; Wu, L.Z.; Ma, L.; Xiong, J.; Wang, B. Effects of local damage on vibration characteristics of composite pyramidal truss core sandwich structure. *Compos. Part B* **2014**, *62*, 73–87. [CrossRef]
9. Xiong, J.; Ma, L.; Pan, S.; Wu, L.; Papadopoulos, J.; Vaziri, A. Shear and bending performance of carbon fiber composite sandwich panels with pyramidal truss cores. *Acta Mater.* **2012**, *60*, 1455–1466. [CrossRef]

10. Wang, B.; Zhang, G.Q.; He, Q.L.; Ma, L.; Wu, L.Z.; Feng, J.C. Mechanical behavior of carbon fiber reinforced polymer composite sandwich panels with 2-D lattice truss cores. *Mater. Des.* **2014**, *55*, 591–596. [CrossRef]

11. Huang, W.; Fan, Z.H.; Zhang, W.; Liu, J.Y.; Zhou, W. Impulsive response of composite sandwich structure with tetrahedral truss core. *Compos. Sci. Technol.* **2019**, *176*, 17–28. [CrossRef]

12. Yin, S.; Wu, L.Z.; Yang, J.S.; Ma, L.; Nutt, S. Damping and low-velocity impact behavior of filled composite pyramidal lattice structures. *J. Compos. Mater.* **2014**, *48*, 1789–1800. [CrossRef]

13. Zhang, G.Q.; Wang, B.; Ma, L.; Wu, L.Z.; Pan, S.D.; Yang, J.S. Energy absorption and low velocity impact response of polyurethane foam filled pyramidal lattice core sandwich panels. *Compos. Struct.* **2014**, *108*, 304–310. [CrossRef]

14. Chen, K.; Neugebauer, A.; Goutierre, T.; Tang, A.; Glicksman, L.; Gibson, L.J. Mechanical and thermal performance of aerogel-filled sandwich panels for building insulation. *Energy Build.* **2014**, *76*, 336–346. [CrossRef]

15. Li, F.M.; Lyu, X.X. Active vibration control of lattice sandwich beams using the piezoelectric actuator/sensor pairs. *Compos. Part B* **2014**, *67*, 571–578. [CrossRef]

16. Song, Z.G.; Li, F.M. Aeroelastic analysis and active flutter control of nonlinear lattice sandwich beams. *Nonlinear Dyn.* **2014**, *76*, 57–68. [CrossRef]

17. Chai, Y.Y.; Li, F.M.; Song, Z.G.; Zhang, C.Z. Analysis and active control of nonlinear vibration of composite lattice sandwich plates. *Nonlinear Dyn.* **2020**, *102*, 2179–2203. [CrossRef]

18. Vakakis, A.F. Inducing passive nonlinear energy sinks in vibrating systems. *J. Vib. Acoust.* **2001**, *123*, 324–332. [CrossRef]

19. Gendelman, O.V.; Starosvetsky, Y.; Feldman, M. Attractors of harmonically forced linear oscillator with attached nonlinear energy sink. I: Description of response regimes. *Nonlinear Dyn.* **2008**, *51*, 31–46. [CrossRef]

20. Starosvetsky, Y.; Gendelman, O.V. Attractors of harmonically forced linear oscillator with attached nonlinear energy sink. II: Optimization of a nonlinear vibration absorber. *Nonlinear Dyn.* **2008**, *51*, 47–57. [CrossRef]

21. Georgiades, F.; Vakakis, A.F. Dynamics of a linear beam with an attached local nonlinear energy sink. *Commun. Nonlinear Sci. Numer. Simul.* **2007**, *12*, 643–651. [CrossRef]

22. Lu, Z.; Wang, Z.X.; Zhou, Y.; Lu, X.L. Nonlinear dissipative devices in structural vibration control: A review. *J. Sound Vib.* **2018**, *423*, 18–49. [CrossRef]

23. Moslemi, A.; Khadem, S.E.; Khazaee, M.; Davarpanah, A. Nonlinear vibration and dynamic stability analysis of an axially moving beam with a nonlinear energy sink. *Nonlinear Dyn.* **2021**, *104*, 1955–1972. [CrossRef]

24. Liu, Y.; Chen, G.P.; Tan, X. Dynamic analysis of the nonlinear energy sink with local and global potentials: Geometrically nonlinear damping. *Nonlinear Dyn.* **2020**, *101*, 2157–2180. [CrossRef]

25. Taghipour, J.; Dardel, M. Steady state dynamics and robustness of a harmonically excited essentially nonlinear oscillator coupled with a two-DOF nonlinear energy sink. *Mech. Syst. Signal Process.* **2015**, *62*, 164–182. [CrossRef]

26. Fang, X.; Wen, J.H.; Yin, J.F.; Yu, D.L. Highly efficient continuous bistable nonlinear energy sink composed of a cantilever beam with partial constrained layer damping. *Nonlinear Dyn.* **2017**, *87*, 2677–2695. [CrossRef]

27. Zang, J.; Yuan, T.C.; Lu, Z.Q.; Zhang, Y.W.; Ding, H.; Chen, L.Q. A lever-type nonlinear energy sink. *J. Sound Vib.* **2018**, *437*, 119–134. [CrossRef]

28. Tian, W.; Li, Y.M.; Li, P.; Yang, Z.C.; Zhao, T. Passive control of nonlinear aeroelasticity in hypersonic 3-Dwing with a nonlinear energy sink. *J. Sound Vib.* **2019**, *462*, 114942. [CrossRef]

29. Li, W.K.; Wierschem, N.E.; Li, X.H.; Yang, T.J.; Brennan, M.J. Numerical study of a symmetric single-sided vibro-impact nonlinear energy sink for rapid response reduction of a cantilever beam. *Nonlinear Dyn.* **2020**, *100*, 951–971. [CrossRef]

30. Zhang, Y.W.; Yuan, B.; Fang, B.; Chen, L.Q. Reducing thermal shock-induced vibration of an axially moving beam via a nonlinear energy sink. *Nonlinear Dyn.* **2017**, *87*, 1159–1167. [CrossRef]

31. Yao, H.L.; Cao, Y.B.; Ding, Z.Y.; Wen, B.C. Using grounded nonlinear energy sinks to suppress lateral vibration in rotor systems. *Mech. Syst. Signal Process.* **2019**, *124*, 237–253. [CrossRef]

32. Chen, J.E.; He, W.; Zhang, W.; Yao, M.H.; Liu, J.; Sun, M. Vibration suppression and higher branch responses of beam with parallel nonlinear energy sinks. *Nonlinear Dyn.* **2018**, *91*, 885–904. [CrossRef]

33. Wei, Y.M.; Wei, S.; Zhang, Q.L.; Dong, X.G.; Peng, Z.K.; Zhang, W.M. Targeted energy transfer of a parallel nonlinear energy sink. *Appl. Math. Mech.* **2019**, *40*, 621–630. [CrossRef]

34. Zhang, Y.W.; Zhang, Z.; Chen, L.Q.; Yang, T.Z.; Fang, B.; Zang, J. Impulse-induced vibration suppression of an axially moving beam with parallel nonlinear energy sinks. *Nonlinear Dyn.* **2015**, *82*, 61–71. [CrossRef]

35. Zhang, Z.; Ding, H.; Zhang, Y.W.; Chen, L.Q. Vibration suppression of an elastic beam with boundary inerter-enhanced nonlinear energy sinks. *Acta Mech. Sin.* **2021**, *37*, 387–401. [CrossRef]

36. Mao, X.Y.; Ding, H.; Chen, L.Q. Bending vibration control of pipes conveying fluids by nonlinear torsional absorbers at the boundary. *Sci. China-Technol. Sci.* **2021**, *64*, 1690–1704. [CrossRef]

37. Wang, G.X.; Ding, H.; Chen, L.Q. Performance evaluation and design criterion of a nonlinear energy sink. *Mech. Syst. Signal Process.* **2022**, *169*, 108770. [CrossRef]

38. Wang, G.X.; Ding, H. Mass design of nonlinear energy sinks. *Eng. Struct.* **2022**, *250*, 113438. [CrossRef]

39. Chen, J.E.; Zhang, W.; Sun, M.; Yao, M.H.; Liu, J. Free vibration analysis of composite sandwich plates with different truss cores. *Mech. Adv. Mater. Struct.* **2018**, *25*, 9701–9713. [CrossRef]
40. Chen, J.E.; Zhang, W.; Sun, M.; Yao, M.H.; Liu, J. Parametric study on nonlinear vibration of composite truss core sandwich plate with internal resonance. *J. Mech. Sci. Technol.* **2016**, *30*, 4133–4142. [CrossRef]